ELSEVIER

Chemical Geology 191 (2002) 89–104

CHEMICAL GEOLOGY
INCLUDING
ISOTOPE GEOSCIENCE

www.elsevier.com/locate/chemgeo

X-ray diffraction study of brabantite–monazite solid solutions

Jean-Marc Montel [a,*], Jean-Luc Devidal [b], Daniel Avignant [c]

[a] LMTG Université Paul Sabatier-CNRS, 39 allées J. Guesde, 31000 Toulouse, France
[b] LMV Université Blaise Pascal-CNRS, 5 rue Kessler, 63000, Clermont-Ferrand, France
[c] LMI Université Blaise Pascal-CNRS, Campus des Cézeaux, 63177, Aubière, France

Abstract

We synthesized compounds with stoichiometry of natural brabantite $M^{2+}Th(PO_4)_2$ with M^{2+} = Ca, Cd, Sr, Pb, Ba at 1 bar, 1200 °C and 2.5 kbar, 700 °C. Those compounds were studied by powder X-ray diffraction and electron microprobe. For Ca, Sr, and Pb, we obtained always crystals with the monazite structure. For Cd, the monazite structure is obtained at 1 bar, but not at 2.5 kbar. For Ba, we obtained the monazite structure only at 2.5 kbar. The unit-cell parameters of the compounds with monazite structure vary regularly with the size of the M^{2+} ion. We studied also the solid-solution $LaPO_4$–$M^{2+}Th(PO_4)_2$, at 1200 °C, 1 bar. The solid solutions for Cd, Ca, and Sr are continuous, and the unit-cell parameters vary linearly with the degree of substitution. For Pb, the solid solution is continuous, but the unit-cell parameters do not vary linearly. For Ba, there is a miscibility gap, with a maximum of about 50 mol% of $BaTh(PO_4)_2$ in $LaPO_4$. These results have several consequences for U–Th–Pb geochronology of monazite, and for utilization of monazite as a nuclear-waste ceramic.

Keywords: Monazite; Brabantite; X-ray diffraction; Geochronology; Nuclear waste

1. Introduction

Monazite, the natural light-rare-earth phosphate is one of the most important accessory minerals in geochemistry. It is widely used in conventional geochronology (Parrish, 1990), because of its commonly high uranium content (commonly 0.05–3 wt.%), and in chemical dating because of its high thorium content (Montel et al., 1996). Monazite is also the main bearer of the Sm–Nd isotopic system in the continental crust and is potentially important for other isotopic systems such as Lu–Hf or La–Ba. Monazite is also known to control the REE behaviour in many crustal systems. It is a widely distributed mineral, from deep crust to sediments. Recently, monazite-based ceramics have been proposed as nuclear waste matrix, mainly for actinides (Boatner and Sales, 1988). The chemistry of the monazite group is complex and can be described by at least 19 end-members: the 14 rare earth phosphates $REEPO_4$, the U- and Th-silicates ($USiO_4$, $ThSiO_4$), two brabantite-like end-members [$CaTh(PO_4)_2$, $CaU(PO_4)_2$], and YPO_4. $USiO_4$ and YPO_4 are not known with monoclinic structure but must be defined as virtual end-members to describe the chemical composition of natural monazite. Additionally, unusual monazite-group minerals have been described that contain high concentrations of Ba and Sr (Chakhmouradian and Mitchell, 1998; Motta de Toledo et al., 1999). Brabantite is the name given to the naturally

* Corresponding author.
E-mail address: montel@cict.fr (J.-M. Montel).

0009-2541/02/$ - see front matter © 2002 Elsevier Science B.V. All rights reserved.
PII: S0009-2541(02)00150-X

occurring end-member $CaTh(PO_4)_2$ (Rose, 1980), synonymous with cheralite (Bowie and Horne, 1953).

The structure of monazite, space group $P2_1/n$, has been refined by Ni et al. (1995) on single crystals. It consists of chains, parallel to the *c*-axis, of alternating PO_4 tetrahedra and the larger site (Fig. 1), into which all the large ions are incorporated (REE, Ca, Th, U). Monazite structure is the normal structure for the bigger REE, from $LaPO_4$ to $TbPO_4$, whereas the zircon structure is preferred by smaller REE, from $TbPO_4$ to $LuPO_4$, and YPO_4, forming xenotime.

In monazite, natural actinides are incorporated through two well-documented substitutions (Cuney and Friedrich, 1987; Förster, 1998): a huttonite-like substitution: $Ln^{3+} + P^{5+} = An^{4+} Si^{4+}$ and a brabantite-like substitution $2Ln^{3+} = An^{4+} Ca^{2+}$ (An for actinides, Ln for lanthanides).

This paper focuses on the brabantite-like substitution: we systematically investigated the replacement of Ca^{2+} in brabantite by other M^{2+} ions: Ba^{2+}, Sr^{2+}, Cd^{2+}, Pb^{2+}. Both end-members and monazite ($LaPO_4$)–brabantite solid solutions were investigated.

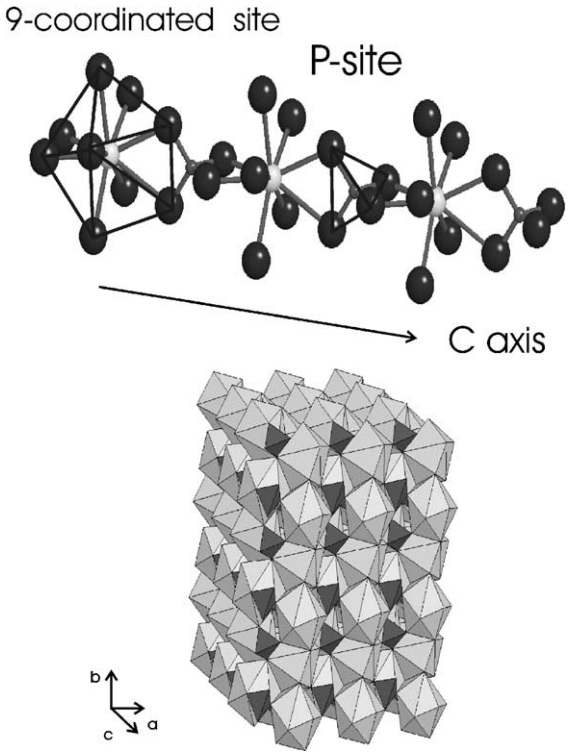

Fig. 1. The monazite structure, from the data of Ni et al. (1995).

2. Experimental procedure

2.1. Preparation of starting materials

The purpose of this study was to obtain products with the brabantite-like formula $M^{2+}Th(PO_4)_2$, as well as brabantite–$LaPO_4$ solid solutions. Three methods were used.

- The simplest starting material was a stoichiometric mixture of nitrates (La, Pb, Sr, Cd, Th), carbonates (Ca) and $(NH_4)_2HPO_4$. These compounds decompose and react at high temperatures. Unfortunately, this easy method is not suitable for hydrothermal synthesis.
- The second method consisted of the mixing of previously synthesized phosphate gels of the various cations. Nitrate or carbonate of the desired cation was dissolved in water, then the phosphate ion was added as an aqueous solution of $(NH_4)_2HPO_4$, leading to the instantaneous formation of a gel. This gel was then rinsed, dried, and fired at 800 °C to eliminate the excess of N, H, O and C, producing a pure phosphate. The last stage was the mixing in stoichiometric proportions of these fired anhydrous phosphates.
- The third method, which was used extensively in this study, is an all-gel method derived from that proposed by Luth and Ingamels (1963). Aliquots of titrated nitrate or carbonate aqueous solutions, matching the targeted brabantite–monazite composition, were mixed together. A gel is formed by the addition of the desired amount of an aqueous solution of $(NH_4)_2HPO_4$. The gel was then rinsed, dried and fired at 700–800 °C. Thus, several grams of a homogeneous and reactive product is obtained in a single step.

2.2. Experiments

Two types of synthesis experiments were performed. The first experimental series was carried out in a one-atmosphere large furnace. The starting material was put into a Pt crucible and allowed to react at 1200 °C for 24 h. All other hydrothermal syntheses are carried out in conventional cold-seal vessels in

gold or platinum crucible as described in detail by Vielzeuf and Montel (1994).

3. Analytical procedure

3.1. X-ray analyses

3.1.1. Data collection.

The solid phases recovered at the end of each run were characterized by X-ray powder diffraction with the use of a Sigma 2080 diffractometer and Cu Kα1 (use of incident-beam monochromator). Forty milligrams of powder was loaded on a sample holder as a randomly oriented powder. For unit-cell parameters, powder X-ray diffraction data were collected in step-scan mode with a step of 0.02° 2Θ and a counting time of 6 s (per step). The 2Θ range was either from 4° to 80° or from 4° to 100° 2Θ. In this latter procedure, Si was used as an internal standard.

3.1.2. Data processing

The digital X-ray patterns were processed using the Fullprof2k Retvield refinement software (Rodriguez-Carvajal, 1990), operating in profile-matching mode. A Gaussian/Lorentzian function was employed for the profile shapes. The peak width (FWHM) was varied as a function of 2Θ using the Caglioti formula and a peak asymmetry correction function was used below 35° 2Θ. Thus, the adjustable parameters were: the zero position, the unit-cell values, the Caglioti function's parameters, the Gaussian/Lorentzian ratio, and two parameters for peak asymmetry. In multiphase patterns, the zero position and the asymmetry parameters are common to all phases, but the other parameters were different. With this procedure, excellent statistical indicators are obtained with a limited number of adjustable parameters. When Si is added as an internal standard, the pattern is processed as a multiphase pattern, with the Si unit-cell parameter fixed at 5.43088 Å. Typically, the statistical precision on cell parameters is better than 0.001 Å at 2Θ and better than 0.01° for angles. The statistical precision reflects only the internal coherency of the data. The accuracy of cell parameters can be estimated only by a calibration procedure, using a standard. Here we used Si as an internal standard, as explained above. The comparison between the calibrated patterns, the non-calibrated patterns, and literature data shows that even for non-calibrated data, the accuracy is around 0.01 Å (Table 2). In multiphase patterns (e.g. in the Mat58 to Mat67 series), the profile-fitting procedure is sometimes difficult, because of peak overlapping problems. Consequently, the quality of these unit-cell parameters is uncertain.

3.2. Microprobe analyses

The compositions of brabantite–monazite solid solutions were analyzed by electron microprobe. Analyses of Sr-, Cd-, Ca-, and Pb-based solid solution were carried out in Toulouse on a CAMECA SX 50 electron microprobe with peak counting time of 20 s at a beam current of 20 nA. All analyses were conducted at 15 kV and ZAF corrections were applied. $LaPO_4$, ThO_2, CdS, a SiO_2–Al_2O_3–CaO–PbO glass, wollastonite, and $SrTiO_3$ were used as La, Th, Cd, Pb, Ca and Sr standards, respectively. For Ba-based solid solutions, the analyses were performed in Clermont-Ferrand on a CAMECA SX 100 electron microprobe. Wollastonite, barite, ThO_2, and YPO_4 were used as Ca, Ba, Th and Y standards, respectively. Analyses were conducted at 15 kV, 20 nA with a counting time of 20 s. Again, ZAF corrections were applied to the analyses.

4. Results

Table 1 summarizes the synthesis conditions and describes the phases obtained. Table 2 reports the brabantite unit-cell parameters and Table 3 the unit-cell parameters of other phases. Finally, Table 4 gives the electron-probe analyses.

4.1. End-members

4.1.1. X-ray patterns

The compounds $SrTh(PO_4)_2$, $PbTh(PO_4)_2$, and $CaTh(PO_4)_2$ always gave an X-ray pattern similar to that of monazite structure. The succession of peaks and the intensities are identical, and the whole pattern can be indexed on a monazite-type unit cell. Only the unit-cell parameters changed. Therefore, we consider that those compounds have a true monazite structure, with a random distribution of M^{2+} and Th^{4+} in the 9-coordinated site. We will refer to those compounds as brabantite–(Ca), –(Pb), –(Sr). For $CdTh(PO_4)_2$, a

Table 1
Summary of experimental results

Run no.	Starting products	Starting composition	Experimental conditions	Results
Mat09	phosphates	Ba	2500 bar, 700 °C, 7 days	brabantite–(Ba) + $Th_2P_2O_7$
Mat10	phosphates	Ca	2500 bar, 700 °C, 7 days	brabantite–(Ca)
Mat11	phosphates	Cd	2500 bar, 700 °C, 7 days	triclinic brabantite–(Cd)
Mat12	phosphates	Pb	2500 bar, 700 °C, 7 days	brabantite–(Pb)
Mat24	phosphates	Sr	2500 bar, 700 °C, 7 days	brabantite–(Sr)
Mat28	nitrates	Ca	1 bar, 1200 °C, 24 h	brabantite–(Ca)
Mat38b	phosphates	Ba	2500 bar, 700 °C, 7 days	brabantite–(Ba)
Mat39	phosphates	Ca	2500 bar, 700 °C, 7 days	brabantite–(Ca)
Mat40	phosphates	Cd	2500 bar, 700 °C, 7 days	brabantite–(Cd)
Mat41	phosphates	Pb	2500 bar, 700 °C, 7 days	brabantite–(Pb)
Mat42	phosphates	Sr	2500 bar, 700 °C, 7 days	brabantite–(Sr)
Mat49	nitrates	Ba	1 bar, 1200 °C, 24 h	X2-brabantite–(Ba)
Mat50	nitrates	Pb	1 bar, 1200 °C, 24 h	brabantite–(Pb)
Mat51	nitrates	Sr	1 bar, 1200 °C, 24 h	brabantite–(Sr)
Mat52	nitrates	Cd	1 bar, 1200 °C, 24 h	brabantite–(Cd)
Mat58	nitrates	La	1 bar, 1200 °C, 24 h	monazite–(La)
Mat59	nitrates	3/4 La–1/4 Ba	1 bar, 1200 °C, 24 h	brabantite solid solution
Mat60	nitrates	1/2 La–1/2 Ba	1 bar, 1200 °C, 24 h	brab s.s. + ThO_2 + $Ba_7Th(PO_4)_6$
Mat61	nitrates	1/4 La–3/4 Ba	1 bar, 1200 °C, 24 h	brab s.s. + X2-brab–(Ba)+ ThO_2+ $Ba_7Th(PO_4)_6$
Mat62	nitrates	Ba	1 bar, 1200 °C, 24 h	X2-Ba–brabantite–(Ba)
Mat63	gel	Ba	1 bar, 1200 °C, 24 h	X2-Ba–brabantite–(Ba)
Mat64	gel	1/4 La–3/4 Ba	1 bar, 1200 °C, 24 h	brab s.s. + X2-brabantite–(Ba)
Mat65	gel	1/2 La–1/2 Ba	1 bar, 1200 °C, 24 h	brab s.s. + X2-brabantite–(Ba)
Mat66	gel	3/4 La–1/4 Ba	1 bar, 1200 °C, 24 h	brabantite solid solution
Mat67	gel	La	1 bar, 1200 °C, 24 h	monazite–(La)
Mat68	gel	La	1 bar, 1200 °C, 24 h	monazite–(La)
Mat69	gel	Sr	1 bar, 1200 °C, 24 h	brabantite solid solution
Mat70	gel	Sr 4/5–La 1/5	1 bar, 1200 °C, 24 h	brabantite solid solution
Mat71	gel	Sr 3/5–La 2/5	1 bar, 1200 °C, 24 h	brabantite solid solution
Mat72	gel	Sr 2/5–La 3/5	1 bar, 1200 °C, 24 h	brabantite solid solution
Mat73	gel	Sr 1/5–La 4/5	1 bar, 1200 °C, 24 h	brabantite solid solution
Mat74	gel	Pb	1 bar, 1200 °C, 24 h	brab s.s. + $Pb_{0.9}Th_{1.8}(PO_4)_3$
Mat75	gel	Pb 4/5–La 1/5	1 bar, 1200 °C, 24 h	brabantite solid solution
Mat76	gel	Pb 3/5–La 2/5	1 bar, 1200 °C, 24 h	brabantite solid solution
Mat77	gel	Pb 2/5–La 3/5	1 bar, 1200 °C, 24 h	brabantite solid solution
Mat78	gel	Pb 1/5–La 4/5	1 bar, 1200 °C, 24 h	brabantite solid solution
Mat79	gel	Cd 1/5–La 4/5	1 bar, 1200 °C, 24 h	brabantite solid solution
Mat80	gel	Cd 2/5–La 3/5	1 bar, 1200 °C, 24 h	brabantite solid solution
Mat81	gel	Cd 3/5–La 2/5	1 bar, 1200 °C, 24 h	brabantite solid solution
Mat82	gel	Cd 4/5–La 1/5	1 bar, 1200 °C, 24 h	brabantite solid solution
Mat83	gel	Cd	1 bar, 1200 °C, 24 h	brabantite solid solution
Mat84	gel	Ca 1/5–La 4/5	1 bar, 1200 °C, 24 h	brabantite solid solution
Mat85	gel	Ca 2/5–La 3/5	1 bar, 1200 °C, 24 h	brabantite solid solution
Mat86	gel	Ca 3/5–La 2/5	1 bar, 1200 °C, 24 h	brabantite solid solution

Table 1 (*continued*)

Run no.	Starting products	Starting composition	Experimental conditions	Results
Mat87	gel	Ca 4/5–La 1/5	1 bar, 1200 °C, 24 h	brabantite solid solution
Mat88	gel	Ca	1 bar, 1200 °C, 24 h	brabantite solid solution
Mat94	nitrates	La	1 bar, 1200 °C, 240 h	monazite–(La)
Mat95	gel	Pb 1/5–La 4/5	2500 bars, 800 °C, 12 days	brabantite solid solution
Mat96	gel	Pb 2/5–La 3/5	2500 bars, 800 °C, 12 days	brabantite solid solution
Mat97	gel	Pb 3/5–La 4/5	2500 bars, 800 °C, 12 days	brabantite solid solution
Mat98	gel	Pb 4/5–La 4/5	2500 bars, 800 °C, 12 days	brabantite solid solution
Mat99	gel	Pb	2500 bars, 800 °C, 12 days	brabantite solid solution

The starting composition is the mole proportion of M^{2+} brabantite and monazite–(La) in the starting mixture; brab. s.s. means brabantite solid solution.

pattern similar to monazite was obtained only at 1 bar [brabantite–(Cd)], but for experiments carried out at 2.5 kbar, another structure is obtained. This pattern can be indexed on a triclinic unit cell, and then this compound is referred to as triclinic brabantite–(Cd). We found the opposite situation for $BaTh(PO_4)_2$. This compound has a monazite structure only when synthesized at 2.5 kbar [brabantite–(Ba)], whereas at 1 bar, another structure was obtained, which can be indexed on a monoclinic unit cell. This is referred to as ''doubled brabantite–(Ba)'' [X2–brabantite–(Ba)], because of its large unit cell (see below).

4.1.2. Unit-cell parameters

The measured unit-cell parameters are in agreement with those previously reported in the literature. For example, the unit-cell parameters of $LaPO_4$ in various experiments ($a=6.825–6.830$ Å, $b=7.062–7.067$ Å, $c=6.497–6.501$ Å, $\beta=103.25–103.28°$) are very close to those determined by Ni et al. (1995) on monocrystals ($a=6.831$ Å, $b=7.075$ Å, $c=6.503$ Å, $b=103.27°$). The most reliable data are, of course, those extracted from the patterns with internal standards. If we consider as an example only the a parameter, we found for brabantite–(Ca) $a=6.695$ Å from the calibrated pattern and $a=6.697$, 6.714, 6.697 Å for other patterns, similar to $a=6.713$ Å for PDF reference 31-0311 and to the $a=6.706$ Å value of Podor and Cuney (1997). The only real disagreement is for run Mat74, which gave $a=6.831$ Å, $b=7.057$ Å, $c=6.549$ Å, $\beta=103.694$ Å, different from the calibrated pattern Mat12Si: $a=6.848$ Å, $b=7.081$ Å, $c=6.565$ Å, $\beta=103.800$ Å. We cannot explain this discrepancy, but we note that the X-ray pattern of Mat74 was not easy to index because it included another monoclinic phase.

The unit-cell parameters of all our brabantite samples display a regular evolution with the variation of the M^{2+} ion size from the smallest brabantite–(Cd), $V=284$ Å^3, up to the biggest brabantite–(Ba), $V=325$ Å^3. If we calculate for each brabantite an average large-ion radius, defined as the mean of the ionic radius of Th and M^{2+} ions, the unit cell parameters a, b, c and the cubic root of the volume follow linear arrays (Fig. 2). Such a regular behavior has been also observed for REE phosphates (Ni et al., 1995). We can note in Fig. 2 that the ionic-radius vs. unit-cell parameters relationships for the a parameter are identical in brabantite and in REE phosphate, that for b they are slightly different, but that for c they are markedly different. The variation of β is more difficult to interpret (Fig. 2), and less regular than for true monazite.

The X2–brabantite–(Ba) has a unit-cell volume that is approximately twice that of the true brabantite–(Ba) (642–653 Å^3 vs. 325 Å^3), but the microprobe analyses indicate that this phase has the brabantite stoichiometry. Therefore, we propose that this change in structure results from the ordering of Ba and Th, as already observed in the $CaUTh(PO_4)_2$ system (Dusaussoy et al., 1996).

The triclinic brabantite–(Cd) has a unit-cell volume of 280–282 Å^3, very close to the true braban-

Table 2
Brabantite unit-cell parameters

Run no.	*a*	*b*	*c*	*β*	χ^2	Composition
Mat09Si	6.944	7.161	6.670	102.880(8)	2.59	$BaTh(PO_4)_2$
Mat10Si	6.695	6.907	6.410	103.609(9)	2.40	$CaTh(PO_4)_2$
Mat12Si	6.848	7.081	6.565	103.800(5)	2.04	$PbTh(PO_4)_2$
Mat24Si	6.792	7.017	6.501	103.514(4)	1.55	$SrTh(PO_4)_2$
Mat28Si	6.714	6.921	6.424	103.683(9)	3.90	$CaTh(PO_4)_2$
Mat38b	6.950(2)	7.162(2)	6.675(2)	102.885(9)	2.21	$BaTh(PO_4)_2$
Mat39	6.697(2)	6.900(2)	6.402(2)	103.660(10)	1.56	$CaTh(PO_4)_2$
Mat41	6.849(2)	7.076(2)	6.560(2)	103.793(11)	2.04	$PbTh(PO_4)_2$
Mat42	6.801(2)	7.027(2)	6.510(2)	103.562(10)	1.65	$SrTh(PO_4)_2$
Mat50	6.848(2)	7.078(2)	6.568(2)	103.716(10)	3.43	$PbTh(PO_4)_2$
Mat51	6.791(2)	7.013(2)	6.518(2)	103.515(9)	2.11	$SrTh(PO_4)_2$
Mat52	6.670(3)	6.881(2)	6.390(3)	104.291(15)	1.96	$CdTh(PO_4)_2$
Ba–La						
Mat58	6.830	7.067	6.500	103.275(6)	3.23	$LaPO_4$
Mat59	6.854	7.085	6.538	103.295(6)	1.63	XLa = 0.757
Mat60	6.851	7.075	6.518	103.399(4)	3.09	XLa = 0.808
Mat61	6.856	7.065(2)	6.575(2)	103.080(17)	2.45	XLa = 0.541
Mat64	6.868	7.091	6.562	103.387(6)	1.95	XLa = 0.479
Mat65	6.868	7.094	6.567	103.363(5)	2.15	XLa = 0.521
Mat66	6.849	7.081	6.535(2)	103.306(4)	2.61	XLa = 0.690
Mat67	6.827	7.062	6.499	103.280(5)	2.41	$LaPO_4$
Sr–La						
Mat68	6.825	7.065	6.497	103.258(6)	6.50	$LaPO_4$
Mat69	6.786	7.001	6.498	103.505(4)	3.62	$SrTh(PO_4)_2$
Mat70	6.793	7.021	6.498	103.439(4)	3.44	XLa = 0.202
Mat71	6.801	7.030	6.500	103.383(8)	3.68	XLa = 0.382
Mat72	6.817	7.051	6.501	103.306(8)	2.87	XLa = 0.738
Mat73	6.809	7.039	6.499	103.341(8)	2.40	XLa = 0.562
Pb–La						
Mat74	6.831	7.057	6.549	103.694(5)	3.58	$PbTh(PO_4)_2$
Mat75	6.823	7.054	6.527	103.495(4)	4.88	XLa = 0.322
Mat76	6.823	7.057	6.516	103.392(4)	2.61	XLa = 0.539
Mat77	6.822	7.056	6.508	103.349(5)	3.22	XLa = 0.722
Mat78	6.823	7.058	6.504	103.295(6)	3.12	XLa = 0.801
Cd–La						
Mat79	6.798	7.027	6.474	103.400(6)	3.30	XLa = 0.774
Mat80	6.776	7.001	6.456	103.502(4)	2.23	XLa = 0.613
Mat81	6.740	6.957	6.427	103.702(3)	3.48	XLa = 0.407
Mat82	6.714	6.924	6.407	103.877(6)	2.93	XLa = 0.241
Mat83	6.670	6.879	6.384	104.165(6)	3.60	$CdTh(PO_4)_2$
Ca–La						
Mat84	6.797	7.027	6.479	103.368(5)	2.70	XLa = 0.753
Mat85	6.775	7.000	6.464	103.437(4)	2.71	XLa = 0.603
Mat86	6.756	6.976	6.450	103.521(5)	2.85	XLa = 0.429
Mat87	6.734	6.950	6.435	103.613(6)	3.83	XLa = 0.235

Table 2 (*continued*)

Run no.	*a*	*b*	*c*	*β*	χ^2	Composition
Ca–La						
Mat88	6.697	6.904	6.402	103.712(4)	3.84	$CaTh(PO_4)_2$
Mat94	6.829(2)	7.065(2)	6.501(2)	103.278(8)	2.12	$LaPO_4$
Pb–La						
Mat95	6.825	7.063	6.503	103.288(6)	5.38	*X*La = 0.857
Mat96	6.823	7.060	6.507	103.314(5)	6.48	*X*La = 0.725
Mat97	6.825	7.061	6.517	103.387(6)	8.05	*X*La = 0.519
Mat98	6.830	7.063	6.531	103.501(6)	8.03	*X*La = 0.311
Mat99	6.848	7.073	6.559	103.768(5)	5.33	$PbTh(PO_4)_2$

Distance are in Angstrom units, angles are in degrees. *X*La is the mole fraction of $LaPO_4$ in brabantite, from Table 4. When it is not indicated, the precision is better than ± 1 for 2σ on the last digit. χ^2 is the chi-squared value obtained after the Rietveld procedure. Si means that silicium was used as internal standard.

tite–(Cd) unit cell (284 Å^3). Each parameter, either unit-cell dimension or angle, is also close to the one in true brabantite–(Cd), suggesting that the transition from true brabantite–(Cd) to the triclinic brabantite–(Cd) is based on a limited distortion of the atomic arrangement. For X2–brabantite–(Ba), triclinic bra-

Table 3
Other phases unit-cell parameters

Run no.	Phase	*a*	*b*	*c*	*α*	*β*	*γ*	Comments
Mat 9	$Th_2P_2O_7$	11.595	12.799	7.129				Si
Mat24	$Th_2P_2O_7$	11.603	12.818	7.130				Si
Mat38b	Th_2P2O_7	11.629(4)	12.695(3)	7.238(3)				
PDF 19-370		11.62	12.80	7.12				
Mat11	tric brab–(Cd)	6.606	6.921	6.376	93.098(6)	104.227(6)	88.526(6)	Si
Mat40	tric brab–(Cd)	6.592(2)	6.904(2)	6.357(2)	93.035(16)	104.205(12)	88.515(14)	
Mat60	ThO_2	5.590(1)						
Mat61	ThO_2	5.591(6)						
PDF 42-1462 ICDD	G.I.A.	5.5970						
Mat60	$Ba_7Th(PO_4)_6$	10.528(1)						Solid solution
Mat61	$Ba_7Th(PO_4)_6$	10.607(6)						Solid solution
PDF 33-0180 ICDD	G.I.A.	10.582						
Mat49	X2-Ba–Brab	12.789(4)	5.434(2)	9.456(3)		102.218(9)		
Mat61	X2-Brab–Ba	12.814(2)	5.443(1)	9.472(2)		102.292(12)		
Mat62	X2-Brab–Ba	12.882(3)	5.445(1)	9.369(2)		101.914(12)		
Mat63	X2-Brab–Ba	12.878(3)	5.449(1)	9.384(2)		101.988(10)		
Mat64	X2-Brab–Ba	12.864(2)	5.458(1)	9.391(2)		102.008(6)		
Mat65	X2-Brab–Ba	12.944(2)	5.499(1)	9.390(2)		102.160(20)		
Mat74	$Pb_{0.9}Th_{1.8}(PO_4)_3$	17.414(3)	6.856(1)	8.131(1)		101.354(2)		
Quarton et al., 1984		17.424	6.8734	8.1348		101.295		

Distance are in Angstrom units, angles are in degrees. When it is not indicated, the precision is better than ± 1 for 2σ on the last digit. Si means that silicium was used as internal standard. The PDF data are given for comparison.

Table 4
Electron-probe phase composition and structural formulae

La–Ca					
Run no.	Mat84	Mat85	Mat86	Mat87	Mat88
P_2O_5	29.45	29.25	29.18	29.49	30.24
CaO	2.95	4.95	6.75	9.14	11.92
La_2O_3	53.23	42.89	30.42	16.67	0.05
ThO_2	14.43	22.50	33.87	45.11	58.12
Total	100.05	99.59	100.22	100.42	100.33
P	1.965	1.958	1.952	1.959	1.983
Ca	0.249	0.419	0.571	0.768	0.990
Th	0.259	0.405	0.609	0.805	1.025
La	1.547	1.251	0.887	0.482	0.002
*X*La	0.753	0.603	0.429	0.235	0.001

La–Cd					
Run no.	Mat79	Mat80	Mat81	Mat82	Mat83
P_2O_5	28.76	27.76	27.43	26.71	26.08
CdO	5.64	8.79	14.51	17.92	23.81
La_2O_3	51.93	39.70	26.21	15.12	0.09
ThO_2	12.93	22.62	32.11	40.35	50.77
Total	99.25	98.87	100.26	100.09	100.76
P	1.985	1.977	1.977	1.974	1.973
Cd	0.215	0.346	0.578	0.732	0.996
Th	0.240	0.433	0.622	0.801	1.033
La	0.547	1.251	0.887	0.482	0.002
*X*La	1.561	1.231	0.823	0.487	0.003

La–Sr					
Run no.	Mat69	Mat70	Mat71	Mat72	Mat73
P_2O_5	28.69	28.18	28.35	29.02	29.13
SrO	21.46	17.29	14.05	6.28	11.01
La_2O_3	0.10	13.36	25.84	50.40	39.13
ThO_2	52.64	41.40	32.02	12.93	21.45
Total	101.88	100.23	100.26	98.63	100.72
P	1.973	1.990	1.979	1.989	1.984
Sr	1.047	0.836	0.672	0.295	0.514
Th	1.008	0.786	0.601	0.238	0.393
La	0.003	0.411	0.786	1.505	1.161
*X*La	0.003	0.411	0.786	1.505	1.161

La–Ba						
Run no.	Mat59	Mat60	Mat61	Mat64	Mat65	Mat66
P_2O_5	28.52	29.15	28.42	28.48	28.33	29.36
BaO	7.55	5.77	13.79	13.21	14.33	10.53
La_2O_3	49.41	52.36	33.79	28.31	31.87	43.59
ThO_2	12.73	10.22	22.79	27.12	22.76	13.64
Total	98.21	97.49	98.79	97.11	97.28	97.11
P	2.003	2.023	2.034	2.064	2.054	2.059
Ba	0.245	0.185	0.457	0.443	0.480	0.342

Table 4 (*continued*)

La–Ba

Run no.	Mat59	Mat60	Mat61	Mat64	Mat65	Mat66
Th	0.240	0.191	0.439	0.528	0.443	0.257
La	1.512	1.583	1.054	0.894	1.005	1.332
*X*La	0.757	0.808	0.541	0.479	0.521	0.690

La–Pb

Run no.	Mat95	Mat96	Mat97	Mat98	Mat99	Mat74	Mat75	Mat76	Mat77	Mat78
P_2O_5	28.76	25.30	26.08	23.79	22.41	22.96	25.53	27.15	28.14	28.95
PbO	6.49	12.12	17.86	26.45	35.57	34.89	25.73	18.57	10.63	9.28
La_2O_3	57.24	47.58	31.03	17.42	0.40	0.43	17.86	31.93	44.63	51.21
ThO_2	7.86	14.87	25.38	31.27	41.81	40.64	30.57	22.37	15.24	9.64
Total	100.35	99.87	100.39	98.93	100.19	98.90	99.70	100.01	98.64	99.08
P	1.990	1.906	1.991	1.981	1.990	2.027	2.040	2.036	2.026	2.032
Pb	0.143	0.290	0.434	0.700	1.005	0.979	0.654	0.443	0.244	0.207
Th	0.146	0.301	0.521	0.700	0.998	0.964	0.657	0.451	0.295	0.182
La	1.726	1.561	1.032	0.632	0.015	0.016	0.622	1.043	1.400	1.566
*X*La	0.857	0.725	0.519	0.311	0.008	0.008	0.322	0.539	0.722	0.801

Oxides are in weight percentage, atoms are structural formula calculated on an 8-oxygen basis. *X*La is the mole fraction of $LaPO_4$ end-member calculated as $La/(La+Th+M^{2+})$, where M^{2+} is Ca, Cd, Pb, Sr, or Ba.

$Ba_7Th(PO_4)_6$–$Ba_6La_2(PO_4)_6$

Run no.	Mat60	Mat61	Mat62	Mat65
P_2O_5	24.85	24.82	24.79	25.64
BaO	54.65	56.91	27.19	26.70
La_2O_3	14.35	8.34	0.09	2.09
ThO_2	3.42	8.06	45.97	44.76
Total	97.27	98.14	98.04	99.20
P	6.050	6.069	1.996	2.013
Ba	6.160	6.444	1.014	0.971
Th	0.224	0.530	0.995	0.945
La	1.511	0.882	0.003	0.071
*X*La	0.755	0.441	0.002	0.036

Oxides are in weight percentage, atoms are structural formula calculated on a 24-oxygen basis. *X*La is the mole fraction of $Ba_6La_2(PO_4)_6$, calculated as La/2.

bantite–(Cd), however, a complete structure study would be necessary.

4.2. Solid solutions

4.2.1. Phases

At 1 bar and 1200 °C, which are the conditions we used for studying the $LaPO_4$–brabantite solid solutions, we found a continuous solid solution for brabantite–(Pb), –(Ca), –(Cd), –(Sr) with $LaPO_4$. For brabantite–(Ba) at 1 bar, we found a miscibility gap, which is not surprising, because $BaTh(PO_4)_2$ at 1 bar and 1200 °C is not isostructural with monazite.

In the $LaPO_4$–$BaTh(PO_4)_2$ system, the phase assemblage changes as a function of the starting products. Starting from nitrates, we found, in addition to a partial $LaPO_4$–brabantite–(Ba) solid solution, ThO_2 and a compound close to $Ba_7Th(PO_4)_6$. Starting from a gel, we found a mixture of $LaPO_4$–brabantite–

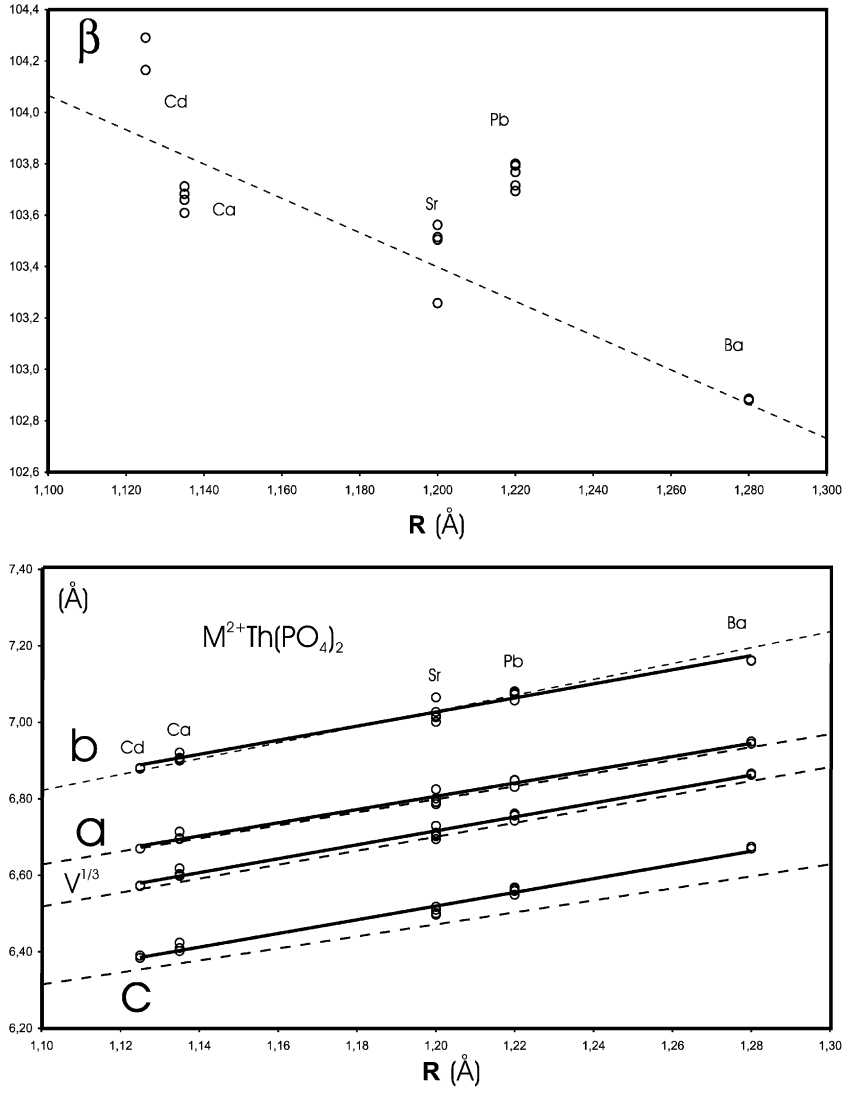

Fig. 2. Evolution of unit-cell parameters for brabantite end-members as a function of the mean ionic radius of the large cation, defined as $(R(M^{2+})+R(Th^{4+}))/2$. The dashed lines represent the equations of Ni et al. (1995) for $LnPO_4$ with the monazite structure.

(Ba) solid solutions with X2–brabantite–(Ba). For this set of data, the electron-probe analyses of phase compositions were necessary to interpret the X-ray patterns. The phase compositions are reported in a Th–La–Ba triangle in Fig. 3. From this diagram, we interpret the results as follows.

For a mole fraction of $BaTh(PO_4)_2$ below 50 mol% in $LaPO_4$ (Mat59, Mat66), a monazite–brabantite solid solution is obtained. If the mole fraction of brabantite–(Ba) in the starting mixture is higher, we obtained a brabantite–(Ba)–$LaPO_4$ solid solution, and Ba and Th which cannot be incorporated in this solid solution form additional phases. These are X2–brabantite–(Ba) if we started from a gel but $ThO_2+Ba_7Th(PO_4)_6$ if we started from nitrate–carbonate mixtures. Several points must be empha-

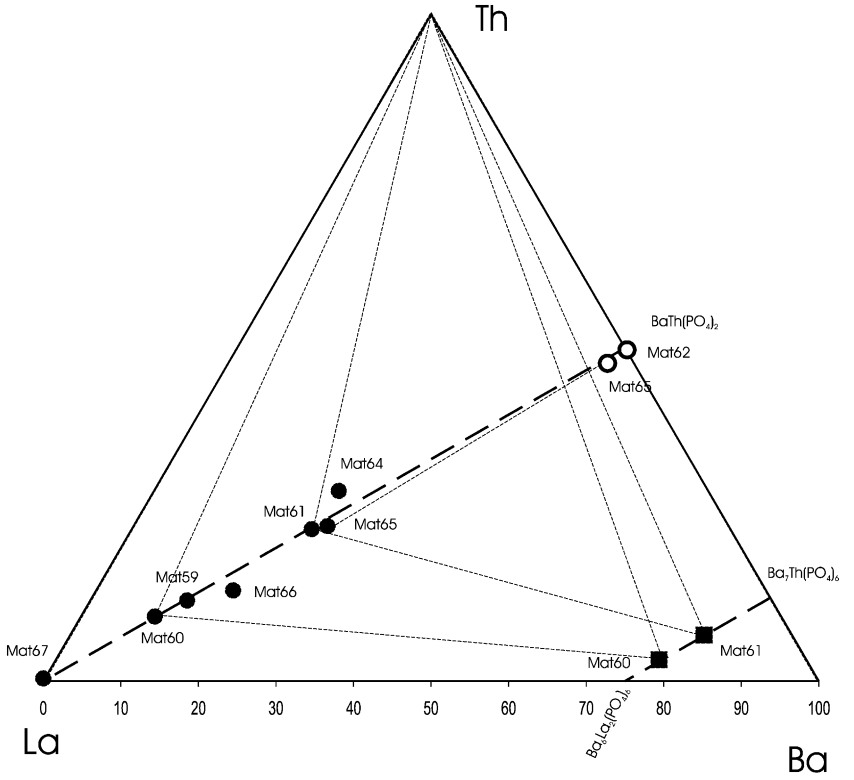

Fig. 3. Phase compositions obtained in the $BaTh(PO_4)_2$–$LaPO_4$ system. Filled circles are brabantite-(Ba)-monazite-(La) solid solutions, empty circles are X2-brabantite–(Ba); squares are $Ba_7Th(PO_4)_6$–$Ba_6La_2(PO_4)_6$ solid solutions.

sized: First, the microprobe data show that the X2–brabantite–(Ba) is always close to the $BaTh(PO_4)_2$ stoichiometry, with very limited La content. Second, there is a limited solid solution from $Ba_7Th(PO_4)_6$ to $Ba_6La_2(PO_4)_6$. This is suggested by the microprobe analyses in Mat60 and Mat61 and by the change in unit-cell parameter of this phase from 10.582 Å for $Ba_7Th(PO_4)_6$ (PDF 33-0180) to 10.607 Å in Mat61 and 10.528 Å in Mat60. Finally, we can estimate the maximum of brabantite–(Ba) that can be incorporated into $LaPO_4$ to be close to 50 mol% (Mat61, Mat64, Mat65) at 1200 °C, 1 bar. However, we must say that the electron probe analyses of the run products are always difficult because most crystals are less than 5 μm in size. For example, it is never possible to obtain pure ThO_2 analysis because this phase is always smaller than the microprobe analytical domain.

4.2.2. Unit-cell parameters

The variations of unit-cell parameters of the various $LaPO_4$–brabantite solid solutions are illustrated in Fig. 4. Brabantite–(Cd), –(Ca), –(Sr)–$LaPO_4$ solid solution displays always a simple behavior. There is a good linear relationship amongst the four unit-cell parameters and volume with the $LaPO_4$ mole fraction. For brabantite–(Ca), our results are similar to the data of Podor and Cuney (1997). For brabantite–(Pb), the unit-cell parameters variations are regular but not linear. This suggests that the $LaPO_4$–brabantite–(Pb) solid solution is continuous but not ideal. The results for Ba are less clear. The parameters a, b, c display regular but non-linear trends. The variation for β is difficult to interpret because the Mat61 and pure brabantite–(Ba) data are not in agreement with the other data.

For phases other than brabantite, the unit-cell parameters are in good agreement with the published

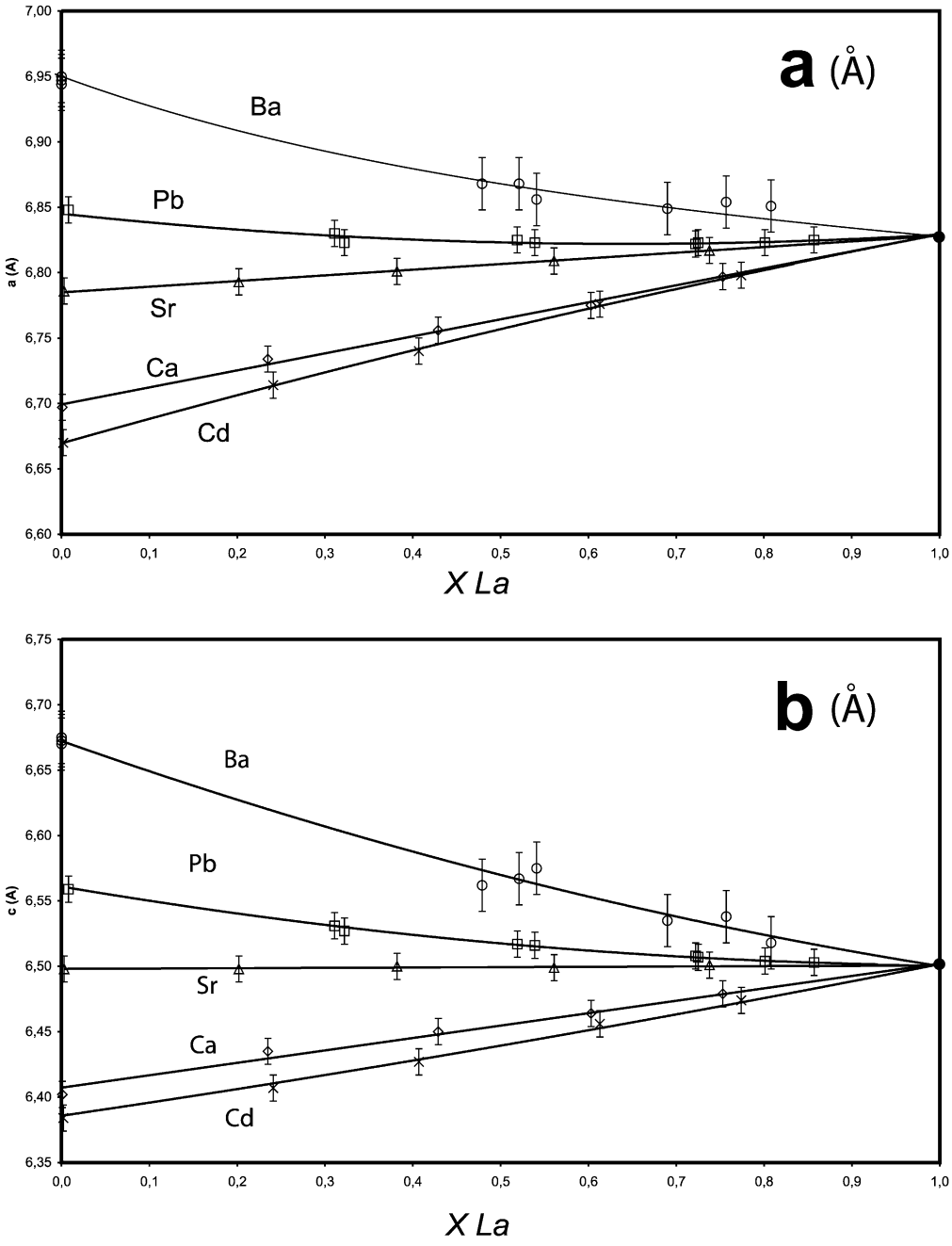

Fig. 4. Variation of unit-cell parameters for brabantite–monazite–(La). Error bars represent 2σ. The lines are hand fitted. *X*La is the mole fraction of $LaPO_4$ in brabantite calculated as $La/(La+M^{2+}+Th)$, where M^{2+} is for Ca, Pb, Sr, Cd, or Ba.

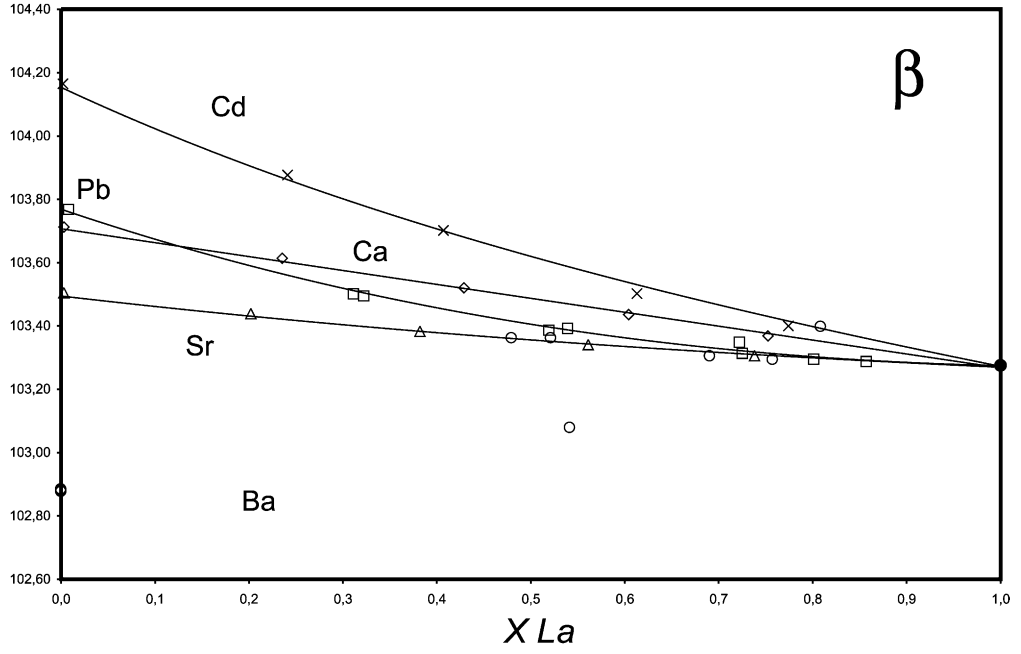

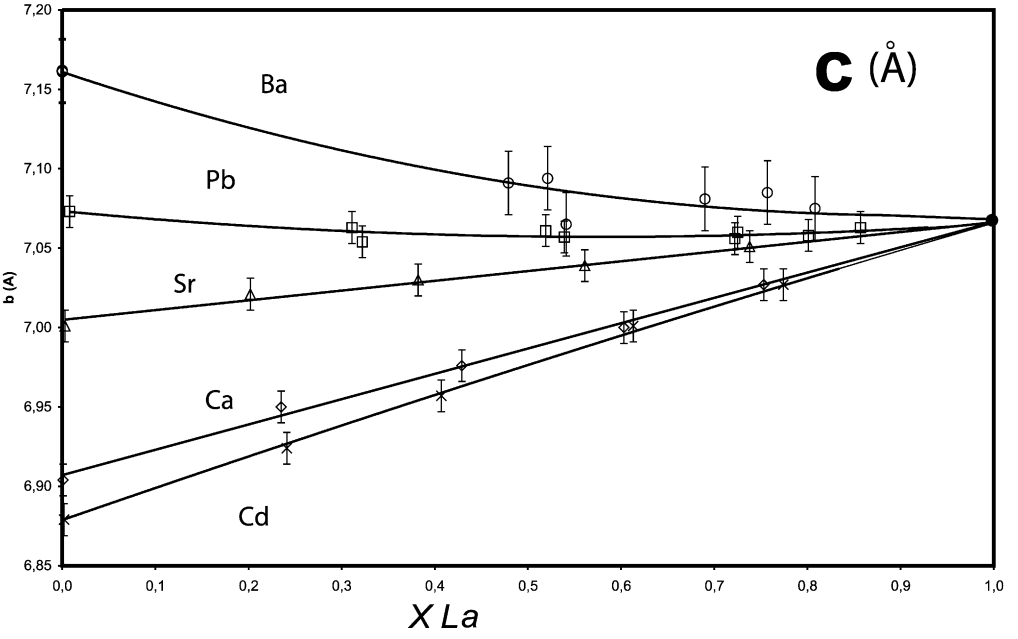

Fig. 4 (*continued*).

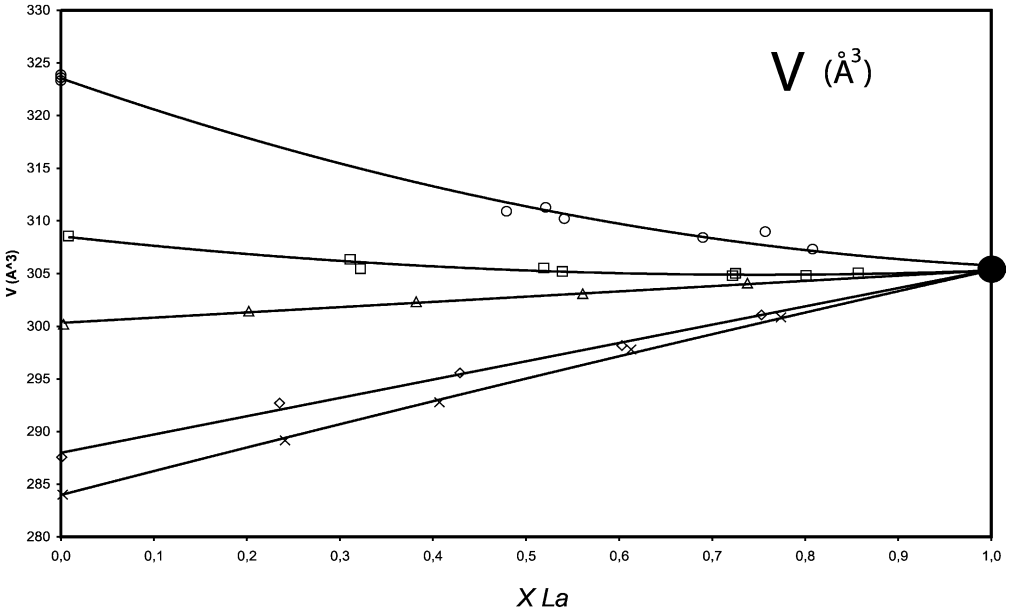

Fig. 4 (*continued*).

values for $Th_2P_2O_7$, for ThO_2, and for $Pb_{0.9}Th_{1.8}(PO_4)_3$ (Table 3).

5. Discussion

5.1. Monazite structure

The monazite structure appears to be an especially accommodating structure, since it can accept ions with variable charges and variable ionic radii. The data for rare-earth phosphates have shown that pure $LnPO_4$ takes the monazite structure from La ($R = 1.216$ Å) to Tb ($R = 1.095$ Å), using the ionic radii of Shannon (1976) in 9-coordination. Here we show that M^{2+} ions from Cd ($R = 1.16$ Å) to Ba ($R = 1.47$ Å) can also be incorporated as major elements. Other compounds are also known to have monazite structure, sometimes with natural occurrences (Carron et al., 1958; Speer, 1980): vanadate, arsenate, chromate, silicates, but also trivalent actinides phosphates $PuPO_4$, $AmPO_4$, $CmPO_4$ (Bjorklund, 1958; Keller and Walter, 1965). The extents of the solid solutions amongst those various compounds are poorly known (see, however, Peiffert and Cuney, 1999, for $LaPO_4$–$ThSiO_4$), but this "softness" of the monazite structure may explain the complex chemical composition of natural monazites.

5.2. Anomalous brabantite and monazite

Recently, several occurrences of unusual monazite composition have been reported. In particular, large amounts of Sr and Ba are compatible with the data presented here (Chakmouradian and Mitchell, 1998; Motta de Toledo et al., 1999). We can anticipate that other natural occurrences of monazite with uncommon compositions will be reported in the future as more studies dealing with accessory minerals are published.

5.3. Geochronology and isotope geochemistry

This paper demonstrates that Pb may occupy a structural site in the monazite structure. The radioactive decay of U and Th produces radiogenic Pb, which can fit in the same site as the parent U or Th. Obviously, because of the displacement occurring during the radioactive decays, the final Pb cannot be

at the same place as the starting U or Th, but this radiogenic Pb will probably occupy the same structural site. This can explain in part the geochronological behavior of monazite. High amounts of radiogenic Pb (above 1 wt.%) have been reported in old radioactive monazite (Montel et al., 1994, Table 1; Montel et al., 1996, Table 4; Cocherie et al., 1998; Braun et al., 1998, Table 5). This may also explain the shielding effect of most minerals relative to the U–Th–Pb system in monazite. For example, it has been shown that monazite included in garnet can stand very high temperatures without losing Pb (Zhu et al., 1994; Montel et al., 2000). To reset of a monazite included in a garnet, the radiogenic Pb of monazite must diffuse through the garnet. Because monazite can accommodate Pb in its structure better than garnet, the partitioning of Pb must be strongly in favor of monazite. Then, the Pb content in monazite will remain higher than in garnet, and draining all Pb out of monazite will take a very long time.

The possibility of incorporating Sr suggests that most monazite should contain some amount of Sr. With the progress of isotopic analytical techniques, we think that it should be possible to extract this Sr from any dated monazite and to analyze its isotopic composition. This could give important information when monazite inheritance is suspected from the U–Pb data (Copeland et al., 1988).

5.4. Nuclear waste

The results of this study have numerous applications for nuclear waste storage. First, the results presented above confirm that monazite can incorporate various ions within its structure. Specifically, monazite can incorporate actinids in the An^{3+} (Am, Cm), or in the An^{4+} (Pu, Np, U, Th), valence state, as well as their various daughter elements. For example, of those elements with half-life greater than 1 day formed within the three natural U–Th–Pb chains, monazite will accommodate all elements except Po, Rn and perhaps Ra. It is unclear whether monazite will incorporate Ra, but because Ba is accepted in large amounts, it seems likely that Ra will also be accommodated, at least in minor amounts. In addition, the possibility for monazite to incorporate Gd and Cd is of interest because both elements are excellent neutron absorbers.

Acknowledgements

This work benefited from support of INSU program "Géomatériaux", and from GRD "Nouvelles Matrices Pour les Dechets". Many thanks to M. Veschambre and Ph. de Parseval for technical help during electron-probe analyses. This paper has been significantly improved by the reviews of Robert Finch, Pete Kinny, and Fritz Finger. Many thanks to John Hanchar for his careful and efficient editorial work, and to Franck Poitrasson who spent a significant time to convince us that this paper had a place in Chemical Geology. **[EO]**

References

Bjorklund, C.W., 1958. The preparation of PuP_2O_7 and $PuPO_4$. J. Am. Chem. Soc. 79, 6347–6350.

Boatner, L.A., Sales, B.C., 1988. Radioactive waste form for the future: monazite. In: Lutze, W., Ewings, R.C. (Eds.), Radioactives Waste Forms for the Future. North Holland, Amsterdam, pp. 495–564.

Bowie, S.H.U., Horne, J.E.T., 1953. Cheralite, a new mineral of the monazite group. Mineral. Mag. 30, 93–99.

Braun, I., Montel, J.M., Nicolet, C., 1998. Electron microprobe dating of monazites from high-grade gneisses and pegmatites from the Kerala Kondalite Belt, southern India. Chem. Geol. 146, 65–85.

Carron, M.K., Mrose, M.E., Murata, K.J., 1958. Relation of ionic radius to structures of rare-earth phosphates arsenates, and vanadates. Am. Mineral. 43, 985–989.

Chakhmouradian, A.R., Mitchell, R.H., 1998. Lueshite, pyrochlore, and monazite–(Ce) from apatite–dolomite carbonatite, Lesnaya Varaka complex, Kola peninsula, Russia. Mineral. Mag. 62, 769–782.

Cocherie, A., Legendre, O., Peucat, J.J., Kouamelan, A.N., 1998. Geochronology of polygenetic monazites constrained by in-situ electron microprobe Th–U-total lead determination: implications for lead behaviour in monazite. Geochim. Cosmochim. Acta 62, 2475–2497.

Copeland, P., Parrish, R.R., Harrison, T.M., 1988. Identification of inherited radiogenic Pb in monazite and its implication for U–Pb systematics. Nature 333, 760–763.

Cuney, M., Friedrich, M., 1987. Physicochemical and crystal-chemical controls on accessory mineral paragenesis in granitoids: implications for uranium metallogenesis. Bull. Mineral. 110, 235–247.

Dusaussoy, Y., Ghermani, N.E., Podor, R., Cuney, M., 1996. Low temperature ordered phase of $CaU(PO_4)_2$. Synthesis and crystal structure. Eur. J. Mineral. 8, 667–673.

Förster, H.J., 1998. The chemical composition of REE-Y-Th-U-rich accessory mineral in peraluminous granites of the Erzgebirge–

Fichtelgebirge region, Germany: Part I. The monazite–(Ce)–brabantite solid-solution series. Am. Mineral. 83, 259–272.

Keller, C., Walter, K.H., 1965. Darstellung, gitterkonstant, un chemische eigenschaften einiger ternarer oxide des plutoniums, americiums, und curium vom typ $Me^{III}X^{V}O_4$. J. Inorg. Chem. 27, 1253–1260.

Luth, W.C., Ingamels, C.O., 1963. Gel preparation of starting materials for hydrothermal experimentation. Am. Mineral. 48, 255–258.

Montel, J.M., Veschambre, M., Nicollet, C., 1994. Datation de la monazite à la microsonde électronique. C. R. Acad. Sci. Paris 318, 1489–1495.

Montel, J.M., Foret, S., Veschambre, M., Nicollet, C., Provost, A., 1996. Electron microprobe dating of monazite. Chem. Geol. 131, 37–53.

Montel, J.M., Kornprobst, J., Vielzeuf, D., 2000. Shielding effect of garnet for the U–Th–Pb system in monazite: example from the Beni-Bousera kinzigites (Morocco). J. Metamorph. Geol. 18, 335–342.

Motta de Toledo, C., Fontan, F., de Oliveira, S.M.B., de Parseval, P., Ribeiro, C.C., 1999. La monacita del macizo alcalino de catalão (Goiás, Brasil), XIXth SEM meeting, Madrid.

Ni, Y., Hugues, J.M., Mariano, A.N., 1995. Crystal chemistry of the monazite and xenotime structures. Am. Mineral. 80, 21–26.

Parrish, R.R., 1990. U–Pb dating of monazite and its application to geological problems. Can. J. Earth Sci. 27, 1431–1450.

Peiffert, C., Cuney, M., 1999. Hydrothermal synthesis of the complete solid solution between monazite ($LaPO_4$) and Huttonite ($ThSiO_4$) at 780 °C and 200 MPa. J. Conf. Abstr. 4, 522.

Podor, R., Cuney, M., 1997. Experimental study of the complete solid solution between $LaPO_4$ and $(Ca_{0.5}Th_{0.5})PO_4$ at $T=780$ °C, $P=200$ MPa. Am. Mineral. 82, 765–771.

Quarton, M., Zouiri, M., Freundlich, W., 1984. Cristallochimie des orthophosphates doubles de thorium et de plomb. C. R. Acad. Sci. Paris 299 (serie II), 785–788.

Rodriguez-Carvajal, J., 1990. "FULLPROF": a program for Rietveld refinement and pattern matching analysis. Abstracts of the Satellite Meeting on Powder Diffraction of the XV Congress of the IUCr, Toulouse, p. 127.

Rose, D., 1980. Brabantite, $CaTh(PO_4)_2$ a new mineral of the monazite group. Neuss. Jahrb. Mineral. Monat. 6, 247–257.

Shannon, R.D., 1976. Revised effective ionic radii and systematic studies of interatomic distances in halides and chalcogenides. Acta Crystallogr., A 32, 751–767.

Speer, J.A., 1980. The actinide orthosilicates. In: Ribbes, P.H. (Ed.), Orthosilicates. Rev. Mineral. vol. 5, 113–135.

Vielzeuf, D., Montel, J.M., 1994. Partial melting of Al-metagreywackes: Part I. Fluid-absent melting experiments and phase relationships. Contrib. Mineral. Petrol. 117, 375–393.

Zhu, X.K., O'Nions, R.K., Belshaw, N.S., 1994. Dating granulite facies metamorphism and depletion: SIMS chronometry of micron-scale monazite inclusions in garnets. Mineral. Mag. 58A, 1004–1005.